Arab J Sci Eng
DOI 10.1007/s13369-016-2236-x

RESEARCH ARTICLE - CIVIL ENGINEERING

Water Surface Profile Computation for Compound Channels with Narrow Flood Plains

B. Naik[1] · **K. K. Khatua**[1]

Received: 7 October 2015 / Accepted: 8 June 2016

Abstract A multivariable regression model has been developed to predict the water surface profile for different compound channels with the non-prismatic flood plain. The nonlinear regression models are developed using relevant experimental data obtained from laboratory experiments. Three sets of laboratory experiments were carried out to exhibit the overbank flow in converging flood plains. The water surface profiles flow measurement was then related to various dimensionless parameters such as converging angle, width ratio and relative distance to develop the model. The results of calculations of water surface profile from the present model show good agreement with the observed data and data of other researchers. Several statistically based analyses were performed to verify the reliability of the developed multivariable regression model.

Keywords Water surface profile · Non-prismatic compound channel · Converging angle · Relative depth

List of symbols

B	Width of compound channel
b	Width of the main channel
h	Height of the main channel
H	Bank full depth
L	Converging length
S	Bottom slope
α	Width ratio (B/b)
δ	Aspect ratio (b/h)
β	Relative depth ($(H-h)/H$))
X_{r}	Relative distance (x/L)
x	Distance between two consecutive sections
θ	Converging angle
Ψ	Non-dimensional water surface profile (H/h)
P_i	Predicted value
O_i	Observed value
MAE	Mean absolute error
MAPE	Mean absolute percentage error
MSE	Mean-squared error
RMSE	Root-mean-squared error

1 Introduction

Rivers play an important role for human civilizations, as we depend upon the river for day-to-day functioning of our life. Due to the continuous use of rivers, larger settlements have grown on the waterway floodplains and made the floodplain convergent. So during the flood, it has resulted in increased loss of life and economic costs due to improper estimation of water surface profile. Generally, natural compound rivers have varying floodplains, so they are called as non-prismatic compound rivers. As natural rivers are non-prismatic in nature, the flow always changes from uniform to non-uniform. Flow modelling in the non-prismatic compound channel is a complex task. Several investigators such as (Sellin [1], Myers and Elsawy [2], Knight et al [3], Khatua et al [4]) have performed extensive research on flow modelling on straight and meandering prismatic compound channels but very less report are found on non-prismatic compound channels. James and Brown [5] investigated that the flow on the expanding floodplain accelerated, whilst the

✉ B. Naik
banditanaik1982@gmail.com

K. K. Khatua
kkkhatua@yahoo.com

[1] Department of Civil Engineering, N.I.T. Rourkela, Rourkela 769008, India

Published online: 25 June 2016

flow on the converging floodplain decelerated. First experiments on converging compound channels with symmetrically narrowing floodplains were performed by Bousmar [6], Bousmar et al. [7] and Rezaei [8] and Rezaei and Knight [9]. These experiments highlighted the geometrical momentum transfer and the associated additional head loss. Proust et al. [10] investigated an asymmetric geometry with a more abrupt convergence. He concluded that larger mass transfer and total head loss resulted from the higher convergence angle (22°). Chlebek et al [11] analysed and compared the flow behaviour of different geometries compound channels namely, skewed channel, symmetrically converging and diverging channels. Recently, Rezaei and Knight [12], Hojjat et al. [13], Naik and Khatua [14] carried out a new experiment on the converging compound channel and produced much more detailed data sets than the previously existing ones. But all the above-mentioned studies have focused on the effect of changes in floodplain sections to evaluate the discharge. The effect of geometry and flow conditions on water surface profile in non-prismatic compound channels has not yet been considered properly. Therefore, a reliable water surface profile modelling is required to identify flooded areas which will be helpful for flood mitigation and risk management study. The effect of contraction of floodplain width on the water depth prediction in a compound channel is now investigated to analyse the dependency of different geometrical and a hydraulic parameter for prediction of water surface profile of a converging compound channel. In the present work, based on the experimental data of National Institute of Technology, Rourkela and Rezaei [8] data, an attempt has been made to develop a reliable mathematical model to predict the water surface profile of compound channel with converging floodplains for different converging angles. The results have been compared well with the observed data sets.

2 Experimental Set-up

Present work on surface water profile of compound channel with converging floodplains has been performed at the Hydraulics and Fluid mechanics Laboratory of Civil Engineering Department of National Institute of Technology, Rourkela, India. All the experiments were carried out in a concrete flume of 15 m long, 0.90 m wide, 0.10 m deep and average bottom slope(s) of 0.0011. Three sets of converging compound channels with varying cross sections were built inside the concrete flume with Perspex sheet. The width ratio of the prismatic part of the channel was $\alpha = 1.8$, and the aspect ratio of the main channel was $\delta = 5$. Keeping the geometry constant, the converging angles of the channels were varied as 12.38°, 9° and 5°, respectively. These have been done to study the effect of converging floodplain angles and water surface profile prediction of converging compound channels. The converging length of the channels was found to be 0.84, 1.26 and 2.28 m, respectively. The roughness of the floodplain and main channel was maintained identical, and the Manning's n was determined as 0.011 from the experimental runs in the channel. Water was supplied to the flume from an underground sump via an overhead tank by series of centrifugal pumps (15 hp capacity each) and recirculated to the sump after flowing through the converging compound channels. A downstream volumetric tank fitted with closure valves for measuring the actual discharge flowing through the channel. An adjustable vertical gate along with flow straighteners was provided in upstream section sufficiently ahead of the head gate to reduce turbulence and velocity of approach. A movable bridge was provided across the flume for both spanwise and streamwise movements of the instrument over the channel area so that each location on the plain of the converging compound channel could be accessed for taking measurements. Series of micro-pitot tubes of 4.77 mm external diameter in conjunction with a suitable vertical manometer and a 16-Mhz Micro-ADV (Acoustic Doppler Velocity-meter) were used to measure longitudinal velocities at a number of locations across the predefined channel section. Water surface depths were measured directly with a point gauge located on an instrument carriage. The flow depth measurements were taken along the centre of the flume at an interval of 0.5 m in both upstream and downstream prismatic parts of the flume and at every 0.1 m in converging part of the flume. Figure 1a shows the plan view of the compound channel with converging floodplains. Figure 1b shows the longitudinal and cross-sectional dimension of the non-prismatic compound channels. Figure 1c shows the non-prismatic compound channel with travelling bridges and flow instruments. Similarly, experiments were conducted by using an 18-m flume at the University of Birmingham, Department of Civil Engineering. A compound channel of simple rectangular cross section was selected, and all experiments were performed in a straight flume, 18 m long, almost 1200 mm wide, 400 mm deep, and with the average bottom slope of 2.003×10^3. Using PVC material, rigid and smooth boundaries were constructed, both for the main channel of 0.398 m width and 0.05 m depth, as also for the floodplains 0.4 m wide. Three sets of experiments were performed in non-prismatic compound channels of convergence angles $\theta = 1.91°$, $\theta = 3.81°$ and $\theta = 11.31°$ [8].

3 Experimental Results

Stage discharge relationship of the starting test reaches prismatic and midsections of non-prismatic part for the different converging compound channel of angle 12.38°, 9°, 5° from in-bank to overbank flow conditions which are shown in Fig. 2a, b, respectively. A total 13-stage discharge runs

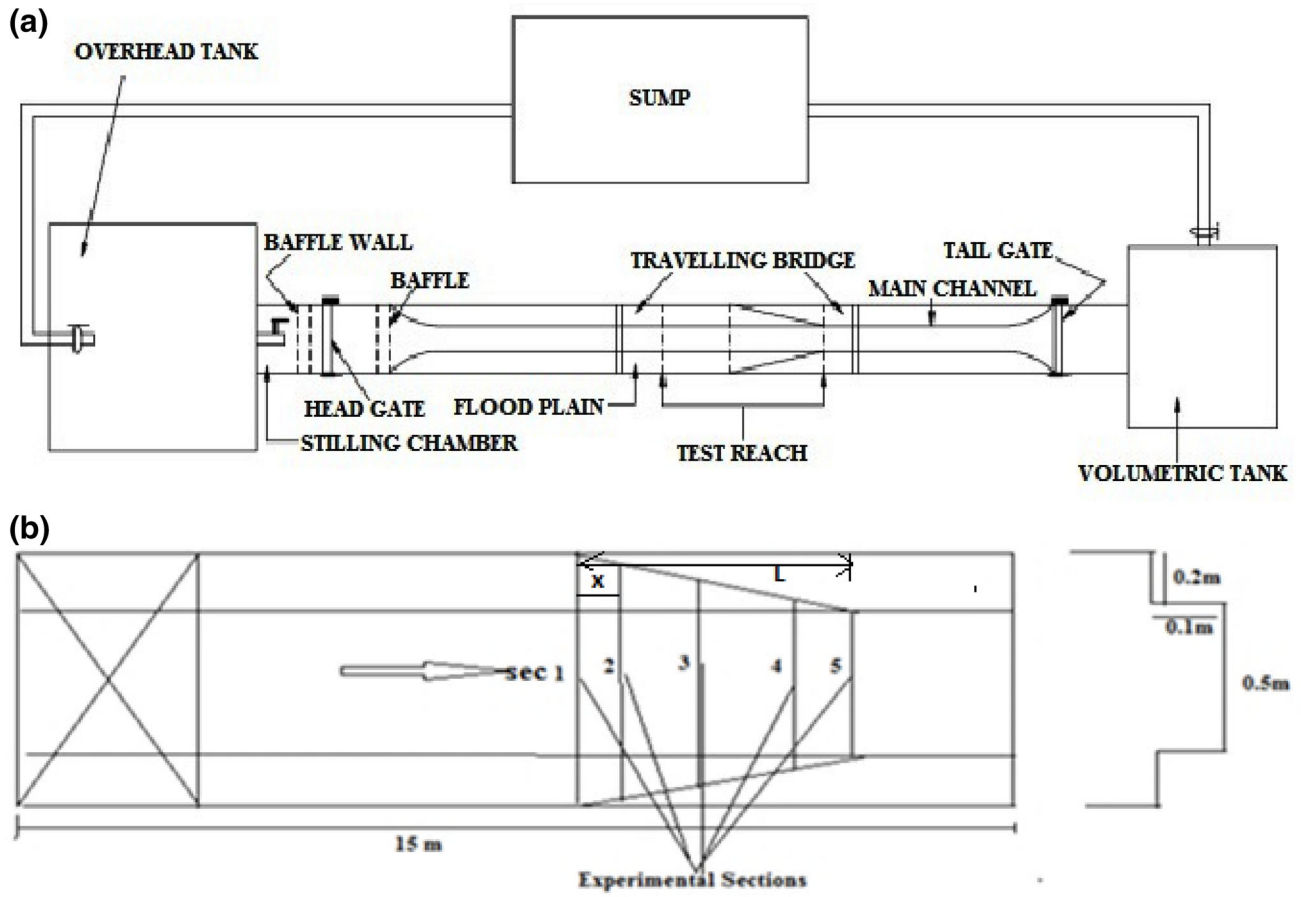

(c)

Fig. 1 **a** Plan view of compound channel with non-prismatic floodplains. **b** Longitudinal and cross-sectional dimension of the non-prismatic compound channels. **c** Non-prismatic compound channel with travelling bridges and flow instruments

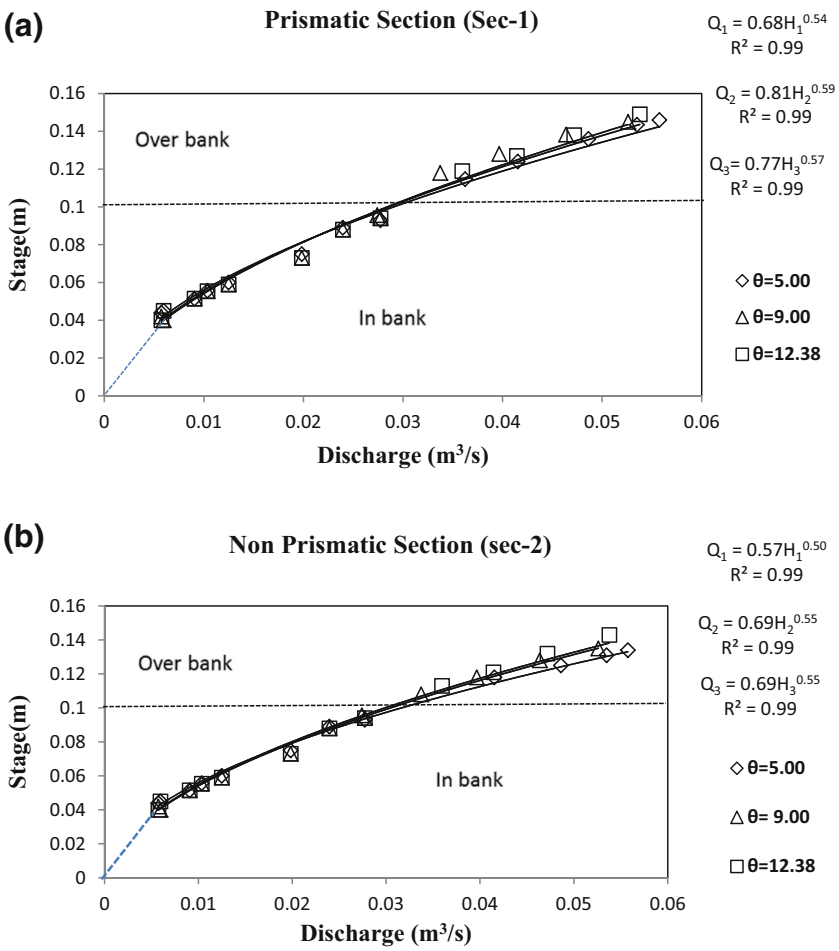

Fig. 2 **a** Stage discharge relationship at the entry of compound channels with converging floodplain of angles 12.38°, 9°, 5° (*prismatic part*) **b** Stage discharge at the middle section of compound channels with converging floodplain of angles 12.38° 9°, 5° (*non-prismatic part*)

of the compound channel with converging flood plains are observed. From Fig 2a, b, we observed that when the converging angle increases for the same stage, discharge also increases. The trends of stage discharge relationships are found to be power functions with high values of R^2 as shown in Fig 2a, b, respectively. Again, all the stage discharge relationships are following the trend $Q = a(H)^n$,where a and n are coefficients as shown in Fig 2a, b. Figure 3a–c shows the water surface profile for different relative depths of different converging floodplains, i.e., 12.38°, 9° and 5°, respectively. It can be noticed from Fig. 3a–c that when the relative distance increases the depth of flow decreases and the decrease is sharp for lower converging angle as compared to higher converging angle. For reference, the typical velocity contour of both prismatic and midsections of non-prismatic part for converging compound channel of angle 12.38° for different flow depths is shown in Fig. 4a, b, respectively. From Fig. 4a, we observed that minimum velocity occurs at the bottom corner of the main channel and floodplain. Maximum velocity occurs at both sides of centreline of the main channel. From Fig. 4b, it can be noticed that maximum velocity occurs at the central region of the main channel.

4 Water Surface Profile Computation and Model Development

An attempt has been made here to model water surface profile for the compound channel with different converging floodplains. The flow can be assumed to be uniform till prismatic part, whereas for the non-prismatic part the flow is found to be non-uniform. Non-dimensional water surface profile has been derived from three different types of converging compound channels fabricated at Hydraulics Laboratory of NIT, Rourkela, India, along with three sets data of Rezaei [8] (details of the data sets are given in Table 1). All these channels have been made homogeneous roughness in both the main channel and floodplain surfaces. Manning's n values for all these smooth surfaces are found to be 0.01. A distinct multiple variable linear regression model has been developed to predict taking five most influencing dimensionless independent parameters. The relationships are expressed as

$$\Psi = F(\alpha, \beta, \delta, \theta, X_r) \text{ for a compound channel with non-prismatic flood plain} \quad (1)$$

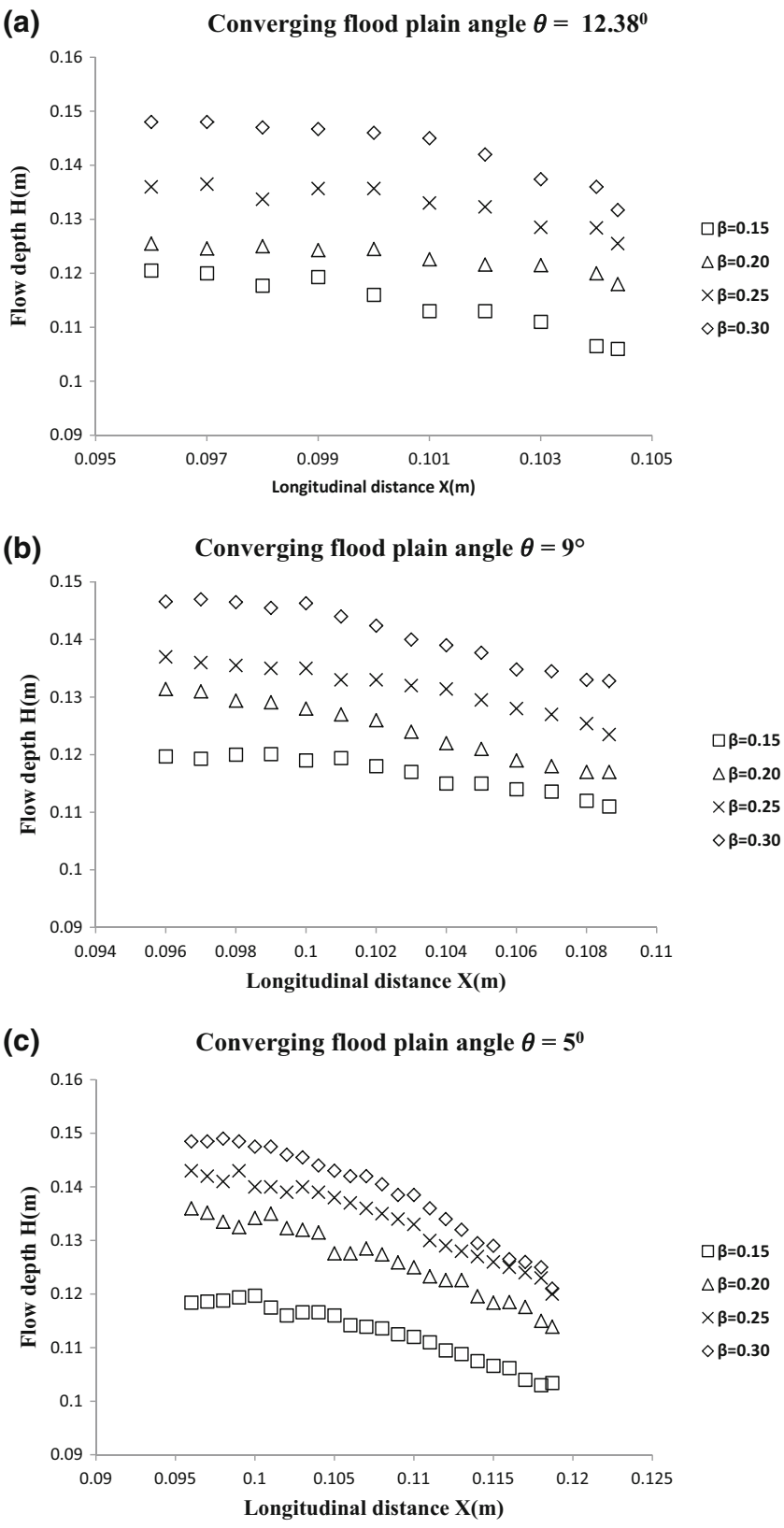

Fig. 3 Water surface profile for compound channel with different converging floodplains for different flow depths (β). **a** 12.38°, **b** $\theta = 9°$, **c** $\theta = 5°$

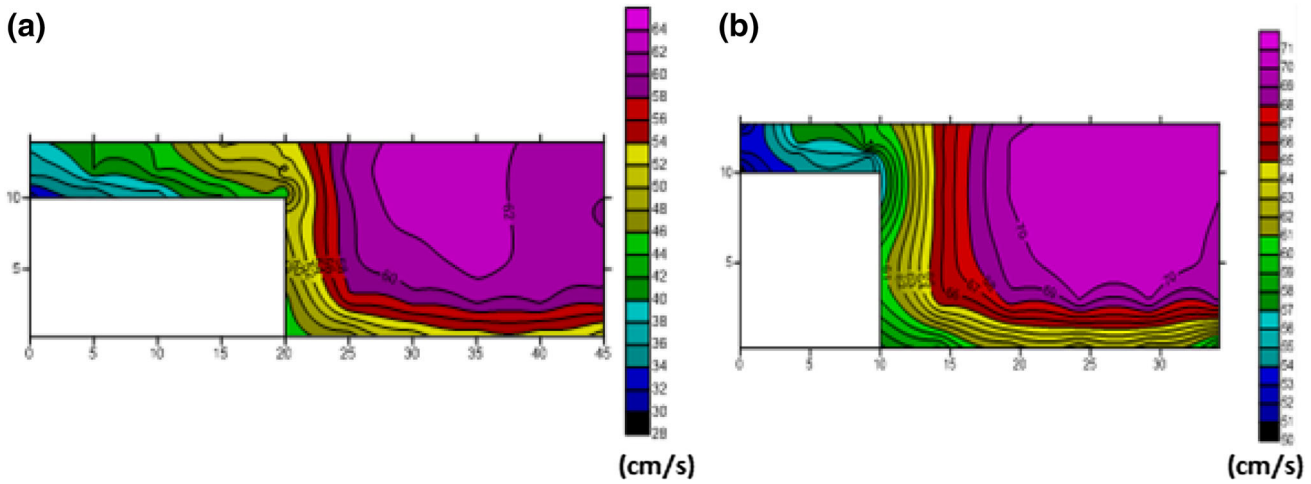

Fig. 4 Velocity contour for compound channel with converging floodplain 12.38°. **a** Prismatic section (sec-1), **b** non-prismatic sections (sec-2) (typical case)

where F represents the functional symbol, α is the width ratio (B/b), β is the relative depth $(H - h/H)$, δ is the channel aspect ratio (b/h), θ is converging angle and X_r is relative distance (x/total non-prismatic length). The independent parameter of β and δ has been chosen from the prismatic part, whereas α, θ and X_r have been chosen from non-prismatic part of the channels. Here, our intension is to predict the non-dimensional water surface profile along the non-prismatic part of the channel. The dependency of non-dimensional water surface profile and the best functional relationships of it have been found out from different plots described below.

4.1 Variation of Non-dimensional Water Surface Profile with Width Ratio α

The variation of non-dimensional water surface profile Ψ in terms of width ratio θ for different converging angles θ is presented in Figs. 5, 6, 7, 8, 9 and 10. Figures 5, 6 and 7 show the variation of water surface profile of converging compound channels of different converging angles of 12.38°, 9°, 5°, respectively. Here, the Ψ has been plotted for four flow discharge cases which bear the relative flow depth β of 0.15, 0.2, 0.25 and 0.3 at the entry of converging part, i.e., prismatic floodplain section (sec-1), respectively. Here, the relative flow depth β at sec-1, i.e., end of the prismatic part of the flood plain, is considered here as reference. The main observation obtained from Figs. 5, 6 and 7 is that for all the discharges, the non-dimensional water surface profile Ψ is found to increase while we travel along the cross-sectional length and along the flow direction. Again, the water surface profile Ψ is found to increase as the relative depth increase. The best fit curves for their relationship are found to be power functions. Figures 8, 9 and 10 show the plot of non-dimensional water surface profile Ψ of non-prismatic part for converging compound channels of the data of Rezaei [8]. Figure 8 is meant for converging angle 11.31°, and Figs. 9 and 10 are for converging angle 3.81° and 1.91°, respectively. The trend of non-dimensional water surface profile Ψ for Rezaei [8] channels is same as NIT Rourkela data. But the best fit curves for Rezaei [8] channels are found to be linear functions because of different aspect ratio and slope of channel.

The fundamental relationships of Ψ with α for different channels of different aspect ratios are presented below. All the equations bear the R^2 value varying between 0.95 and 0.99.

$$\Psi = F_1(\alpha) = 1.06(\alpha)^{0.22} \quad \text{for lower-aspect-ratio channel 1} \tag{2}$$

$$\Psi = F_2(\alpha) = 1.16(\alpha)^{0.22} \quad \text{for lower-aspect-ratio channel 2} \tag{3}$$

$$\Psi = F_3(\alpha) = 1.21(\alpha)^{0.29} \quad \text{for lower-aspect-ratio channel 3} \tag{4}$$

$$\Psi = F_4(\alpha) = 0.07(\alpha) + 1.78 \quad \text{for higher-aspect-ratio channel 1} \tag{5}$$

$$\Psi = F_5(\alpha) = 0.05(\alpha) + 1.28 \quad \text{for higher-aspect-ratio channel 2} \tag{6}$$

$$\Psi = F_6(\alpha) = 0.13(\alpha) + 1.25 \quad \text{for higher-aspect-ratio channel 3} \tag{7}$$

4.2 Variation of Non-dimensional Water Surface Profile with Relative Distance X_r

The effect of relative distance X_r on the non-dimensional water surface profiles has been investigated in this section.

Table 1 Hydraulic parameters for the experimental channel data sets

Verified test channel	Type of channels	Converging angle (Θ)	Longitudinal slope (S)	Cross-sectional geometry	Total channel width (B, m)	Main channel width (b, m)	Main channel depth (h, m)	Width ratio at begining B/b (α)	Converging length ratio (X_r, m)	Aspect ratio b/h (δ)
Rezaei (2006)	Convergent (CV2)	11.31°	0.002	Rectangular	1.2	0.398	0.05	3	2	7.96
Rezaei (2006)	Convergent (CV6)	3.81°	0.002	Rectangular	1.2	0.398	0.05	3	6	7.96
Rezaei (2006)	Convergent (CV6)	1.91°	0.002	Rectangular	1.2	0.398	0.05	3	6	7.96
N.I.T. Rkl	Convergent	5°	0.0011	Rectangular	0.9	0.5	0.1	1.8	2.28	5
N.I.T. Rkl	Convergent	9°	0.0011	Rectangular	0.9	0.5	0.1	1.8	1.26	5
N.I.T. Rkl	Convergent	12.38°	0.0011	Rectangular	0.9	0.5	0.1	1.8	0.84	5

The variation of Ψ in terms of relative distance X_r for different converging angles θ is presented in Figs. 11, 12, 13, 14, 15 and 16. It can be noticed from Figs. 11, 12, 13, 14, 15 and 16 that the water surface profile is found to fall when the relative distance X_r increases. It shows that converging transition increases the velocity head rapidly, hence lowering the potential head. This can also be clarified from velocity contours of Fig. 4a, b. The fall is very high for higher converging floodplain angles. The trends of fall are found to be linear for all the converging compound channels. Rezaei [8] channels provide flatter water surface profile variations as compared to present experimental channels because present experimental channels have low width ratio, i.e., narrow floodplain as compared to Rezaei [8] channels.

Again the relationships of Ψ with X_r for different channels of different aspect ratios are presented below. All equations bear R^2 value varying between 0.93 and 0.99.

$$\Psi = F_7(X_r) = -0.14(X_r) + 1.22 \quad \text{for lower-aspect-ratio channel 1} \tag{8}$$

$$\Psi = F_8(X_r) = -0.15(X_r) + 1.32 \quad \text{for lower-aspect-ratio channel 2} \tag{9}$$

$$\Psi = F_9(X_r) = -0.22(X_r) + 1.37 \quad \text{for lower-aspect-ratio channel 3} \tag{10}$$

$$\Psi = F_{10}(X_r) = -0.15(X_r) + 2.01 \quad \text{for higher-aspect-ratio channel 1} \tag{11}$$

$$\Psi = F_{11}(X_r) = -0.16(X_r) + 1.45 \quad \text{for higher-aspect-ratio channel 2} \tag{12}$$

$$\Psi = F_{12}(X_r) = -0.21(X_r) + 1.67 \quad \text{for higher-aspect-ratio channel-3} \tag{13}$$

Relationships of these non-dimensional parameters with Ψ presented from Eqs. (1) to (12) are attempted to compile to get a generalize expression for Ψ. To achieve this, we have applied all these equations to multilinear regression software and finally six equations are obtained for different converging angles, i.e., (lower-aspect-ratio and higher-aspect-ratio channel 1, 2, 3). The equations are obtained

$$\Psi = F_{13}(\alpha, X_r) = -1.22 + 2.27(\alpha)^{0.22} + 0.18(X_r) \quad \text{for lower-aspect-ratio channel 1} \tag{14}$$

$$\Psi = F_{14}(\alpha, X_r) = -1.21 + 2.28(\alpha)^{0.22} + 0.19(X_r) \quad \text{for lower-aspect-ratio channel 2} \tag{15}$$

$$\Psi = F_{15}(\alpha, X_r) = -0.58 + 1.63(\alpha)^{0.29} + 0.18(X_r) \quad \text{for lower-aspect-ratio channel 3} \tag{16}$$

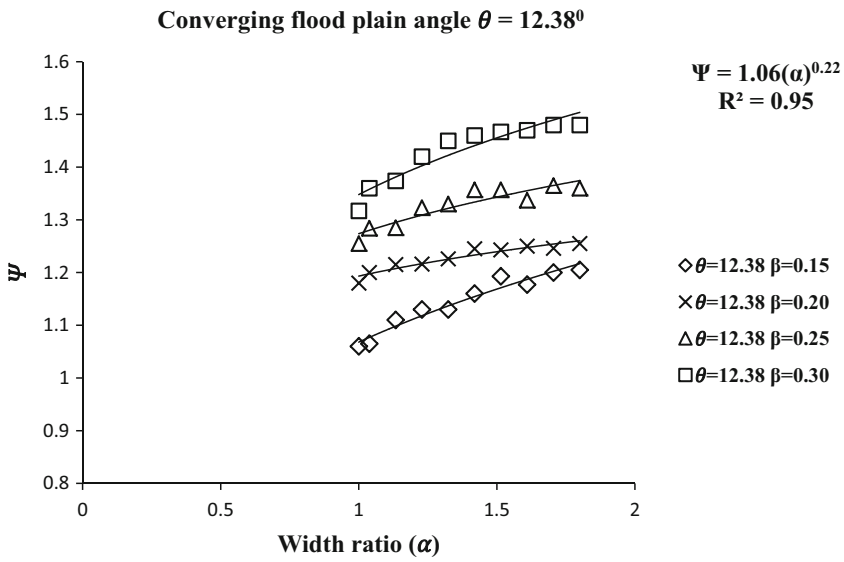

Fig. 5 Variation of water surface profile versus width ratio of different relative depth for converging angle 12.38°

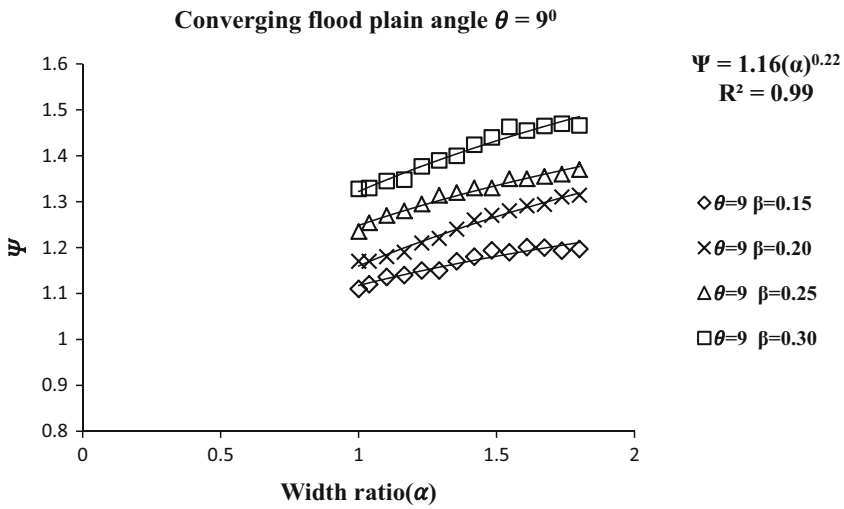

Fig. 6 Variation of water surface profile versus width ratio of different relative depth for converging angle 9°

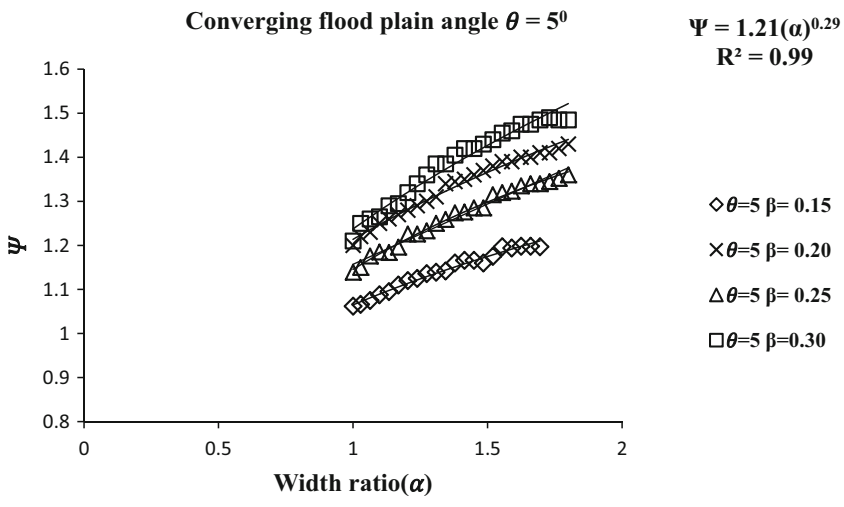

Fig. 7 Variation of water surface profile versus width ratio of different relative depth for converging angle 5°

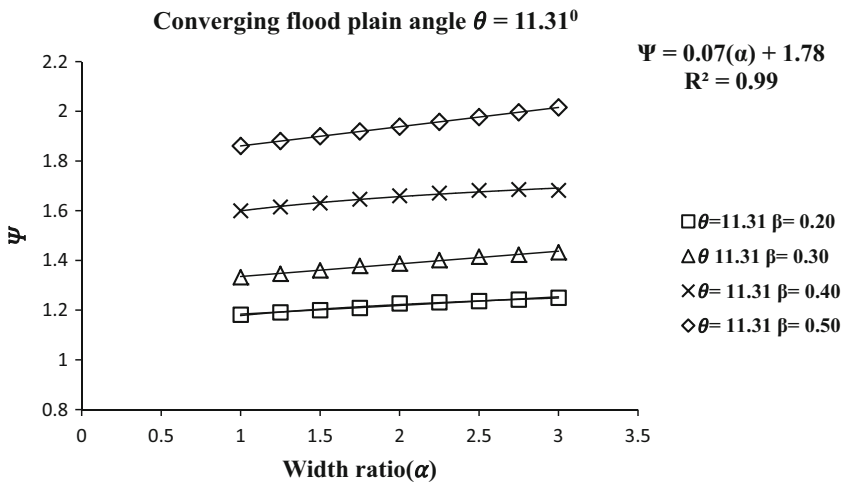

Fig. 8 Variation of water surface profile versus width ratio of different relative depth for converging angle 11.31°

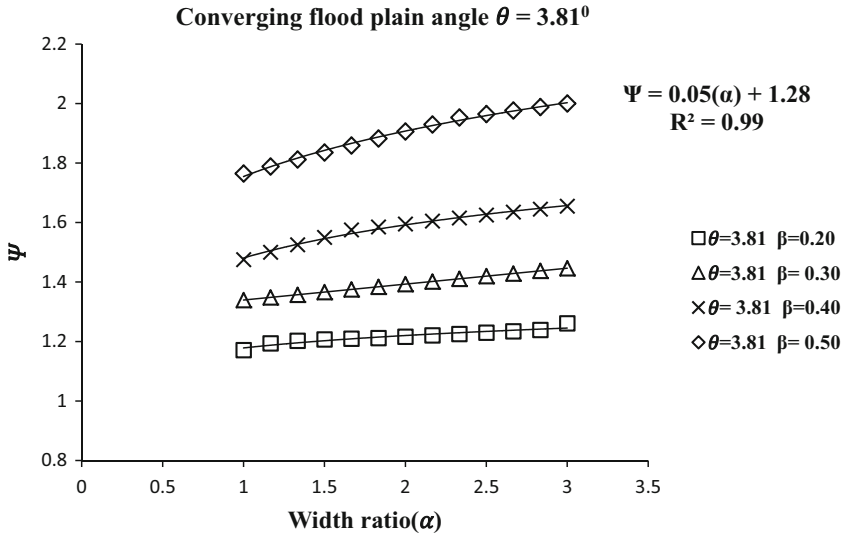

Fig. 9 Variation of water surface profile versus width ratio of different relative depth for converging angle 3.81°

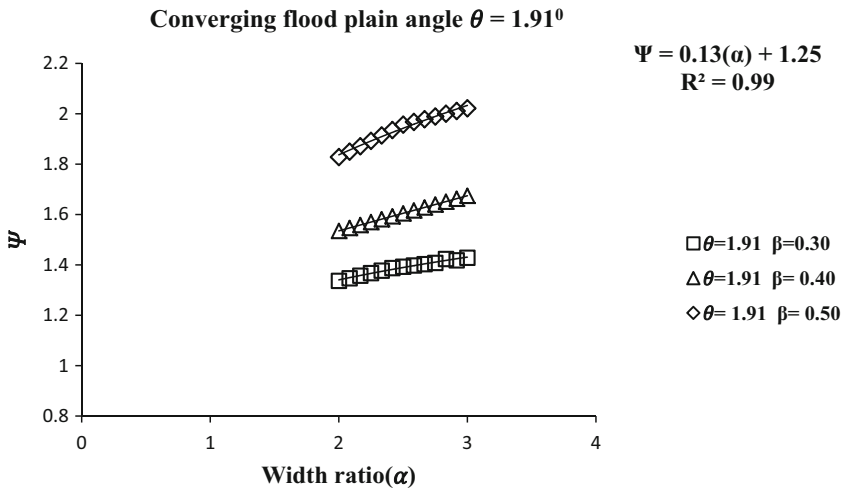

Fig. 10 Variation of water surface profile versus width ratio of different relative depth for converging angle 1.91°

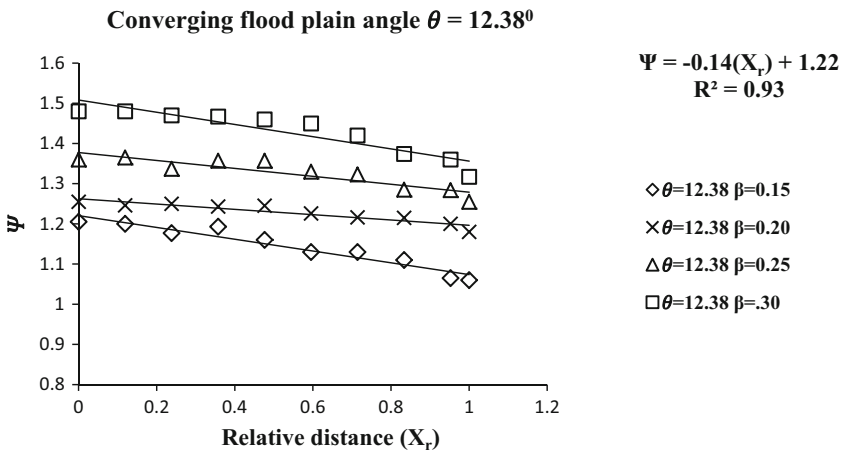

Fig. 11 Variation of water surface profile versus relative distance of different relative depth for converging angle 12.38°

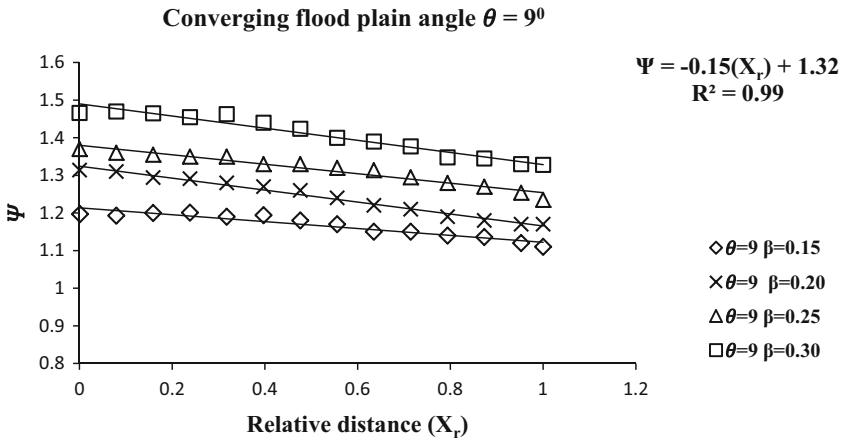

Fig. 12 Variation of water surface profile versus relative distance of different relative depth for converging angle 9°

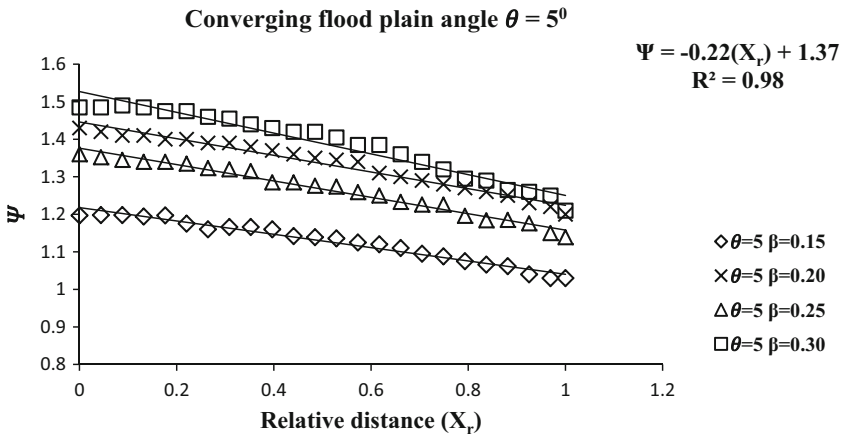

Fig. 13 Variation of water surface profile versus relative distance of different relative depth for converging angle 5°

$$\Psi = F_{16}(\alpha, X_r) = -0.66 + 0.29(\alpha) + 0.12(X_r) \quad \text{for higher-aspect-ratio channel 1} \tag{17}$$

$$\Psi = F_{17}(\alpha, X_r) = 0.86 + 0.29(\alpha) + 0.11(X_r) \quad \text{for higher-aspect-ratio channel 2} \tag{18}$$

$$\Psi = F_{18}(\alpha, X_r) = 0.86 + 0.29(\alpha) + 0.12(X_r) \quad \text{for higher-aspect-ratio channel 3} \tag{19}$$

For lower-aspect-ratio channels, the non-dimensional water surface profile Ψ bears a nonlinear relationship with width ratio α and longitudinal distance X_r, whereas for higher-aspect-ratio cases it provides linear relationship with inde-

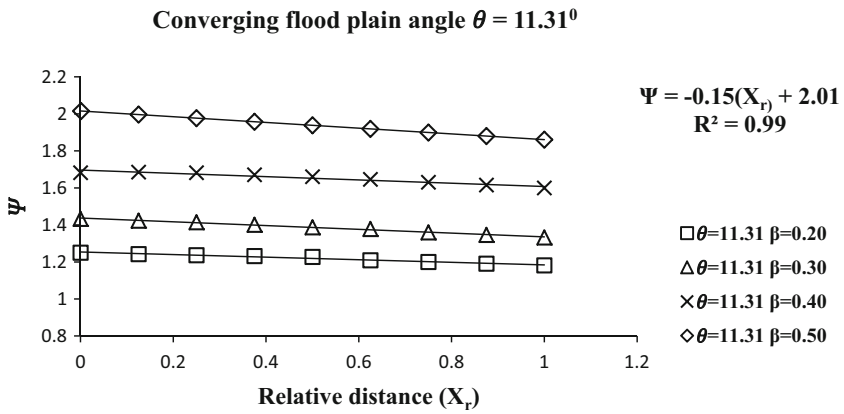

Fig. 14 Variation of water surface profile versus relative distance of different relative depth for converging angle 11.31°

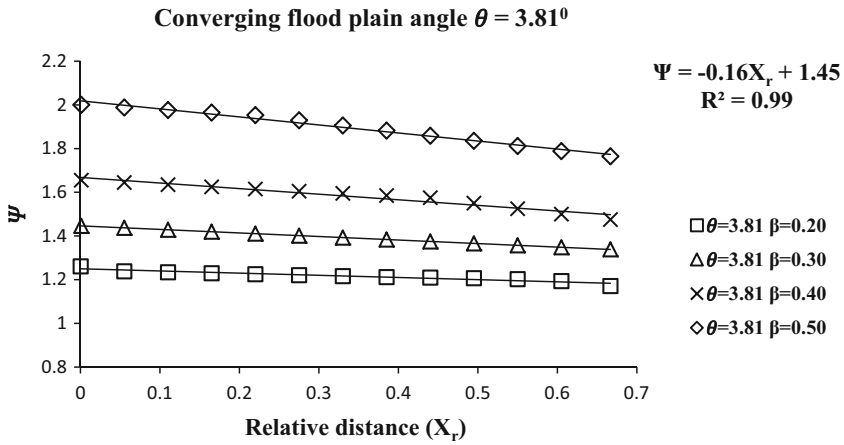

Fig. 15 Variation of water surface profile versus relative distance of different relative depth for converging angle 3.81°

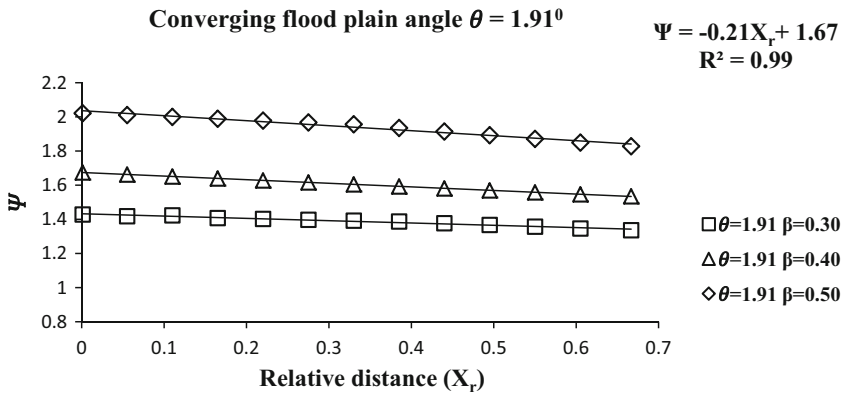

Fig. 16 Variation of water surface profile versus relative distance of different relative depth for converging angle 1.91°

pendent variables. Table 2 provides the total error analysis from Eqs. (13)–(18) obtained from multilinear regression model. The equations bearing least error have been chosen for further improvement of the model.

Table 3 represent the unstandardized coefficient and regression statistics of the regression analysis. The multivariable linear regression techniques have been used to estimate the regression coefficients associated with the derived multivariable regression models after performing the necessary linear transformations of the dimensionless groups. When deriving the generalized empirical models for Ψ as presented in Eq. (13), optimization of 4 main regression statistics was done to arrive at the best possible prediction regression equation. The estimated values of the 4 deployed statistics are provided in Table 3. The corresponding variable coefficient t statistic values are generally high ranging from 3.28 to 25.96 which results in a confidence level of 99.99 %. The empirical prediction models for Ψ presented in Eq. (13) are significant at a confidence level of 99.99 % as the model F-statistic is equal to the value of 541.23 as provided in Table 3. The predictive models have a determination coefficient (R^2) of 0.895. The last statistic used is the model standard error of

Table 2 Detail error analysis of six equations

Sl. no.	Equations	MAPE
Equation 13	$\Psi = -1.22 + 2.27(\alpha)^{0.22} + 0.18X_r$	2.49
Equation 14	$\Psi = -1.21 + 2.28(\alpha)^{0.22} + 0.19X_r$	4.51
Equation 15	$\Psi = -0.58 + 1.63(\alpha)^{0.29} + 0.18X_r$	5.56
Equation 16	$\Psi = -0.66 + 0.29\,(\alpha) + 0.12X_r$	8.61
Equation 17	$\Psi = 0.86 + 0.29\,(\alpha) + 0.114X_r$	7.65
Equation 18	$\Psi = 0.86 + 0.29\,(\alpha) + 0.12X_r$	9.73

estimate which is generally small compared to Ψ the predicted values with its value being equal to 0.043.

An attempt is further made to compile the dependency of Ψ with the effect of converging angle θ which is now discussed in the next section.

4.3 Variation of Non-dimensional Water Surface Profile with Converging Angle θ

Non-dimensional water surface profile (Ψ) is dependent upon the geometry and flow variables. Thus, (Ψ) is found to be varying along the length of the channel and is greatly affected by the variations of converging floodplain angle θ. Our intension is to develop a generalized model taking care of these parameters. Equations (13)–(18) have been found to provide good results for particular converging angles, e.g., Eq. (13) found to provide good results for converging angles θ of 12.38°. Same equation cannot be applied for other converging angle cases; if we applied for other converging angle cases, it provides poor results. This may be due to non-inclusion of converging angle θ. So there is a need for further improvement for the model for incorporating the effect of converging angle θ.

After obtaining six multilinear equations based on geometry, i.e., width ratio α and relative distance X_r, Eq. (13) is found to provide least error. It can be noticed from Fig. 17 that Ψ^* is found to increase when the relative depth increases. The best fit curves for their relationship are found to be an exponential function, and the value of R^2 is found to be 0.94.

$$\Psi^*(\theta) = \frac{\text{Actual } \Psi}{Eq.\ (13)} \tag{20}$$

$$\frac{\text{Actual } \Psi}{Eq.\ (13)} = e^{0.0017\theta} \tag{21}$$

$$\Psi = e^{0.0017\theta}[-1.21 + 2.25(\alpha)^{0.22} + 0.18\,(X_r)] \tag{22}$$

Equation 22 represents the final form of mathematical expression for the water surface profile of a compound channel with the converging flood plain. Similar mathematical model using this multivariable regression model has been done by other researchers, e.g., Bjerkile et al. [15], Dash and Khatua [16]

Table 3 Summary of statistics associated with multivariable regression predictive models

Predicted variable	Model coefficients	Coefficient t statistic	Confidence level (%)	Model F statistic	Model R^2	Model standard error
Intercept	0.33	3.28	99.99	541.23	0.75	0.043
β	1.95	25.96	99.99			
X_r	−1.18	−8.97	99.99			

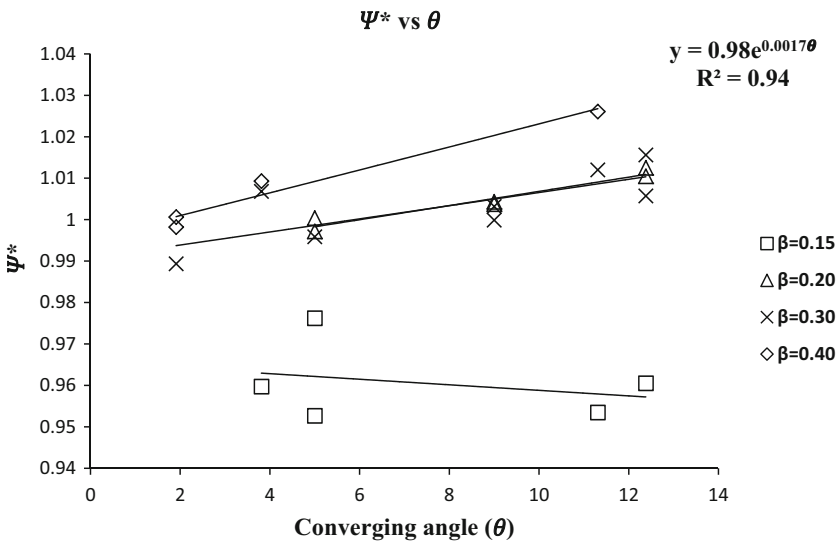

Fig. 17 Variation of Ψ^* versus converging angles (θ) for different relative flow depths (β)

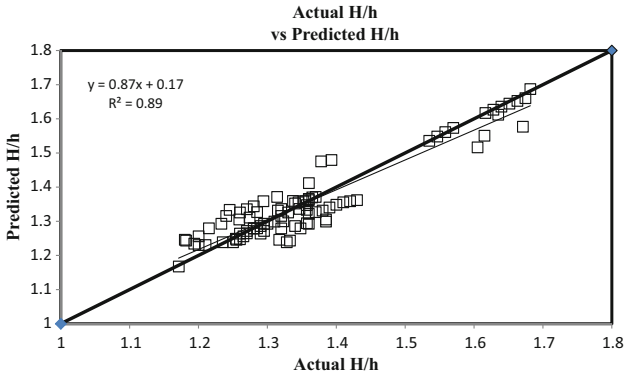

Fig. 18 Scatter plot for observed and modelled value of water surface profile

5 Results and Discussion

5.1 Error Analysis

The variation between the calculated values of water surface profile using Eq. (21) and the corresponding observed values for all the six types of channels is shown in Fig. 18. A regression curve is plotted between observed and calculated values of water surface profile. The present work is a development of a model based on regression analysis, in which around 70 % of data have been used for modelling and 30 % for validation. It can be observed from the data that a high degree of the coefficient of correlation R^2 of 0.89 is obtained, which indicates that the predicted water surface profile is well matching with that of observed values for present experimental channels, as well as Rezaei [8] channels.

To check the strength of the model, error analyses have been done. Mean absolute error (MAE), the mean absolute percentage error (MAPE), mean-squared error (MSE) and the root-mean-squared error (RMSE) for all the converging compound channel for different flow conditions have been estimated. Efficiency criterion like R^2, Nash–Sutcliffe efficiency (E) and index of agreement (I_d) has also been estimated to provide more information on the systematic and dynamic errors present in the model simulation. The definitions of error terms are described below, which have also been used by many researchers such as Dash and Khatua [16]. The detailed results of the error analysis are presented in Table 4.

The expressions used to estimate the various errors include:

1. Mean absolute error (MAE)

The mean absolute error has been evaluated as,

$$\mathrm{MAE} = \frac{1}{n}\sum_{i}^{n}\left|\frac{P_i - O_i}{O_i}\right| \tag{23}$$

Table 4 Different error analysis for Eq. 21

MAE	0.0015
MAPE	2.4296
MSE	0.0019
RMSE	0.0431
E	0.8945
R^2	0.8960
I_d	0.7260

where P_i = predicted values, O_i = observed values

Mean absolute error (MAE) measures how far predicted values are away from observed values. Thus, minimum the deviation of the predicted value from the observed value, better the result will be.

2. Mean absolute percentage error (MAPE)

Mean absolute percentage error is also known as mean absolute percentage deviation. It was usually expressed as a percentage and was defined by the formula

$$\mathrm{MAPE} = \frac{1}{n}\sum_{i}^{n}\left|\frac{O_i - P_i}{O_i}\right| \tag{24}$$

Mean percentage deviation of the predicted value from the observed value is within 10 %; then, the model can be regulated as a good prediction model.

3. Mean-squared error (MSE)

Mean-squared error measures the average of the squares of the errors. It is computed as

$$\mathrm{MSE} = \frac{1}{n}\sum_{i}^{n}(P_i - O_i)^2 \tag{25}$$

The MSE value zero signifies that the estimated data of the observed parameter are likely to be most accurate or ideally best. Since it is difficult to achieve zero value, it is seen that the closest value to zero is reasonably acceptable.

4. Root-mean-squared error (RMSE)

Root-mean-squared error or root-mean-squared deviation is also a measure of the differences between values predicted by a model or an estimator and the actually observed values. These individual differences are called as residuals when the calculations are performed over the data sample that is used for estimation and are known as estimation errors when computed out of the sample. The RMSE is defined as,

$$\mathrm{RMSE} = \sqrt{\mathrm{MSE}} \tag{26}$$

When two data sets, i.e., one set from theoretical prediction and the other from actual measurement of some physical variable (which is in our case is observed versus predicted), are compared, the RMSE of the pairwise deviation among the

two data sets can function as a measure how far on average the error is from 0.

5. Coefficient of correlations R^2

The coefficient of correlation R^2 can be expressed as the squared ratio between the covariance and the multiplied standard deviations of the observed and predicted values. The range of R^2 lies between 0 and 1.0 which describes how much of the observed dispersion is explained by the prediction. A value of zero means no correlation at all, whereas a value of 1 means that the dispersion of the prediction is equal to that of the observation.

6. Nash–Sutcliffe efficiency E

The efficiency E proposed by Nash and Sutcliffe [17] is defined as:

$$E = 1 - \frac{\sum_i^n (O_i - P_i)^2}{\sum_i^n (O_i - \bar{O})^2} \tag{27}$$

where $\bar{O}$ represents the mean of calculated values. The range of E lies between 1.0 (perfect fit) and $-\infty$.

7. Index of agreement I_d

The index of agreement I_d was proposed by Willmot [18]. The index of agreement represents the ratio of the mean square error and the potential error [18] and is defined as:

$$I_d = 1 - \frac{\sum_i^n (O_i - P_i)^2}{\sum_i^n (|P_i - \bar{O} + |O_i - \bar{O}||)^2} \tag{28}$$

The range of I_d is similar to that of R^2 and lies between 0 (no correlation) and 1.0 (perfect fit).

6 Conclusions

From the experimental results on compound channels with converging flood plains, the variation of non-dimensional water surface profile Ψ with relative depth β, converging angle θ, relative distance X_r and width ratio α has been analysed.

The non-dimensional water surface profile Ψ is found to increase with increase in width ratio and relative distance of converging compound channels. Further, the non-dimensional water surface profile Ψ is found to increase exponentially with overbank flow depth for lower-aspect-ratio channels and increase linearly for higher-aspect-ratio channels. Again, the non-dimensional water surface profile Ψ is found to increase when the relative depth increases for different converging angles θ. The dependency of non-dimensional water surface profile Ψ with five most influencing non-dimensional geometric and hydraulic parameters of a converging compound channels is analysed. For all the parameters, it is found to bear the nonlinear relationship.

A multivariable regression model has been presented to model a generalized expression to predict the water surface profile of compound channels with converging flood plains. Different error analyses are performed to test the strength of the present model. It is found that MAE is 0.0015, MAPE is 2.4296 which is less than 10 %, MSE is 0.0019, RMSE is 0.0431, E is 0.8945, R^2 is 0.896, and I_d is 0.726. From these error analyses, it is seen that the present model is capable of predicting confidently the water surface profile with narrowing flood plain.

The limitation of the model is that it can be utilized to predict the water surface profile of compound channel with converging flood plain for homogeneous roughness only. The model can be improved with more data sets from wider flood plains and for differential roughness in the main channel and flood plains.

Acknowledgments The author wishes to acknowledge thankfully the support from the Institute and the UGC UKIERI Research project (ref no UGC-2013 14/017) by the second authors for carrying out the research work in the Hydraulics laboratory at National Institute of Technology, Rourkela.

References

1. Sellin, R.H.J: A laboratory investigation into the interaction between flow in the channel of a river and that of its flood plain. La Houille Blanche **7**, 793–801 (1964)
2. Myers, W.R.C.; Elsawy, E.M.: Boundary shears in channel with flood plain. J. Hydraul. Div. ASCE **101**(7), 933–946 (1975)
3. Knight, D.W.; Tang, X.; Sterling, M.; Shiono, K.; McGahey, C.: Solving open channel flow problems with a simple lateral distribution model. River Flow. **1**, 41–48 (2010)
4. Khatua, K.K.; Patra, K.C.; Mohanty, P.K.: Stage-discharge prediction for straight and smooth compound channels with wide floodplains. J. Hydraul. Eng. ASCE **138**(1), 93–99 (2012)
5. James, M.; Brown; R.J.: Geometric parameters that influence flood plain flow. In: U.S. Army Engineer Waterways Experimental Station. Vicksburg Miss, June, Research report H-77 (1977)
6. Bousmar, D.; Zech, Y.: Periodical turbulent structures in compound channels. In: River Flow International Conference on Fluvial Hydraulics. Louvain-la-Neuve, Belgium, pp. 177–185 (2002)
7. Bousmar, D.; Wilkin, N.; Jacquemart, J.H.; Zech, Y.: Overbank flow in symmetrically narrowing floodplains. J. Hydraul. Eng. ASCE **130**(4), 305–312 (2004)
8. Rezaei, B.: Overbank flow in compound channels with prismatic and non-prismatic floodplains. Ph.D. Thesis. University of Birmingham, UK (2006)
9. Rezaei, B.; Knight, D.W.: Application of the Shiono and Knight Method in the compound channel with non-prismatic floodplains. J. Hydraul. Res. **47**(6), 716–726 (2009)
10. Proust, S.; Rivière, N.; Bousmar, D.; Paquier, A.; Zech, Y.: Flow in the compound channel with abrupt floodplain contraction. J. Hydraul. Eng. **132**(9), 958–970 (2006)
11. Chlebek, J.; Bousmar, D.; Knight, D.W.; Sterling, M.A.: comparison of overbank flow conditions in skewed and converging/diverging channels. In: River Flows International Conference, pp. 503–511 (2010)
12. Rezaei, B.; Knight, D.W.: Overbank flow in compound channels with non prismatic floodplains. J. Hydraul. **137**, 815–824 (2011)

13. Hojjat, A.Y.; Mohammad, H.O.; Seyed, A.A.: The hydraulics of flow in non-prismatic compound channels. J. Civ. Eng. Urban. **3**(6), 342–356 (2013)
14. Naik, B.; Khatua, K.K.; Miri Kamel: Energy loss along the non-prismatic reach of a compound channel using ANN river flow. In: International Conference on Fluvial Hydraulics (September 3–5), Lausanne, Switzerland (2014)
15. Bjerklie, D.M.; Dingman, S.L.; Bolster, C.H.: Comparison of constitutive flow resistance equations based on the Manning and Chezy equations applied to natural rivers. Water Resour. Res. **41**(11), 14 W11502 (2005)
16. Dash, S.S.; Khatua, K.K.: Sinuosity dependency on stage discharge in meandering channels. Am. Soc. Civ. Eng. doi:10.1061/(ASCE)IR.1943-4774.0001037 (2016)
17. Nash, J.E.; Sutcliffe, J.V.: River flow forecasting through conceptual models, part I. A discussion of principles. J. Hydrol. **10**, 282–290 (1970)
18. Willmot, C.J.: On the validation of models. Phys. Geogr. **2**, 184–194 (1981)
19. Khiabani, M.H.; Kandasamy, J.: Friction factor for spatially varied flow with increasing discharge. J. Hydraul. Eng. **131**(9), 792–799 (2005)